Liquid droplet-like behaviour of whole casein aggregates adsorbed on graphite studied by nanoindentation with AFM

Helstad, Kristina; Rayner, Marilyn; van Vliet, Ton; Paulsson, Marie; Dejmek, Petr

Published in:
Food Hydrocolloids

DOI:
10.1016/j.foodhyd.2006.10.006

2007

Available online at www.sciencedirect.com
ScienceDirect
Food Hydrocolloids 21 (2007) 726–738
FOOD HYDROCOLLOIDS
www.elsevier.com/locate/foodhyd

Liquid droplet-like behaviour of whole casein aggregates adsorbed on graphite studied by nanoindentation with AFM

Kristina Helstad[a], Marilyn Rayner[a,*], Ton van Vliet[b], Marie Paulsson[a], Petr Dejmek[a]

[a]*Department of Food Technology, Engineering and Nutrition, Box 124, Lund University, 221 00 Lund, Sweden*
[b]*Wageningen Centre for Food Sciences, P.O. Box 557, 6700 AN Wageningen, The Netherlands*

Received 29 May 2006; accepted 6 October 2006

Abstract

AFM measurements in the force volume mode were performed over the total penetration depth for different positions on casein aggregates adsorbed to a graphite surface in a liquid cell. The stiffness of the force curves was correlated to indentation depths, layer depth and lateral position within the aggregates with the aim of arriving at a credible explanation for the shapes of the force curves. The commonly used Hertz-based models did not fit the experimental data.

The ratio between the height and diameter of the adsorbed casein aggregates was found to be linear, suggesting surface energy dominated liquid droplet behaviour. To investigate the possibility, numerical simulations were performed using the Surface Evolver, an interactive finite element program for the study of surfaces shaped by surface tension and other energies. Simulated force curves were in good agreement with experimental findings, both with respect to slope as a function of indentation as well as describing the variation with indentation position on the aggregate due to interfacial and geometric effects.

By comparing the simulated force curves to the measurement data it was found that there would have been an interfacial energy equivalent to 10 mJ/m^2.

Keywords: Casein; Nanorheology; Adsorption; AFM; Surface evolver; Modelling

1. Introduction

In bovine milk the majority of the proteins are caseins and exist as roughly spherical aggregates called casein micelles. The properties of casein micelles influence to a large extent the technological use of milk, especially in cheese making. Casein and casein micelles have been thoroughly investigated. However, due to the complexity and necessity of stable liquid environment, the exact structure of the casein micelle is not yet known, nor are the rheological properties of single casein micelles. The micellar properties could until recently only be studied by ensemble methods such as light scattering and microscopy methods on dried or frozen samples. Uricanu, Duits, and Mellema (2004) reported the first nanorheological measurements on casein micelles in a liquid environment and found an elastic behaviour for small indentations. However, in previous work (Helstad, Braem, Trckova, Paulsson, & Dejmek, 2004) it was found that the nanorheological properties of casein micelles attached to a graphite surface, measured by atomic force microscopy (AFM) with indentation depths of 20–120 nm, could not be explained by an elastic model. Thus, further investigations and hypotheses are needed to explain the nanorheological behaviour of casein micelles, and to learn more about its internal structure. Here we investigate whether a surface tension based model can describe the nanorheological properties of casein micelles.

1.1. Casein micelle

Casein micelles are formed by associations of the casein components α_{S1}-, α_{S2}-, β-, and κ-casein (Walstra, Geurts, Noomen, Jellema, & van Boekel, 1999). The caseins α_{S1}-, α_{S2}-, and β-casein easily precipitate with Ca^{2+} ions and are

*Corresponding author. Tel.: +46 46 222 4743; fax: +46 46 222 4622.
E-mail address: marilyn.rayner@food.lth.se (M. Rayner).

0268-005X/$ - see front matter © 2006 Elsevier Ltd. All rights reserved.
doi:10.1016/j.foodhyd.2006.10.006

mostly located inside the casein micelle, while κ-casein usually has one phosphate residue per molecule and therefore binds calcium weakly and most of κ-casein is present at the surface of the casein micelle (Dalgleish, 1998). Each micelle consists of between 20,000 to 150,000 casein molecules. The casein micelles are voluminous and contain on average about 4 ml water/g of casein (Walstra et al., 1999). The size range has been established by electron microscopy and dynamic light scattering as 50–500 nm, with an average diameter of ~150 nm (De Kruif & Holt, 2003). Casein micelles have a small negative charge, the ς-potential is 18 mV at 25 °C (Dalgleish, 1984), which provides the electrostatic repulsion between the micelles.

The surface of casein micelles has a flexible diffuse "hairy" layer with a hydrodynamic thickness of 7 nm that is generally assumed to consist of the hydrophilic C-terminal part of κ-casein. This layer could account for the predominantly steric stabilization of casein micelles in dispersion (Holt & Horne, 1996; Walstra, 1979; Walstra, 1990; Walstra et al., 1999). However, β-casein and α-casein may share the surface with κ-casein (Dalgleish, 1998). Dalgleish, Spagnuolo, and Goff (2004) employed the field emission scanning electron microscopy technique to image casein micelles. These images show that the surface of the casein micelles is not smooth. The surface contains gaps between tubular substructures. Dalgleish et al. (2004) suggest that the micelle surface is flexible, consisting of a number of "brushlets" with κ-casein grouped at the ends of the tubules. Partially demineralized casein micelles have been less studied. The demineralization is slow, and will in presence of sufficient Ca at neutral pH only lead to partial disintegration of micelles on a timescale of days, (Aoki, Yamada, & Imamura, 1988; Holt & Horne, 1996; Lucey, Dick, Singh, & Munro, 1997).

Many models for the structure of casein micelles have been proposed. The submicelle model was proposed by Slattery and Evard (1973), Schmidt and Payens (1976) and further developed by Schmidt (1980, 1982) and Walstra (1990, 1999). The basic concept of the model is that the casein micelles consist of an aggregate of discrete spherical subunits (10–20 nm) called submicelles, contained in the interstitial liquid. The subunits are linked together by colloidal calcium phosphate and other electrostatic forces (salt bridges) as well as hydrophobic bonds. This model suggests that the C-terminal part of the κ-casein sticks out from the casein micelle into the solvent as flexible 'hairs' and that this causes a steric repulsion between the casein micelles which protect them from aggregation.

Holt (1992) argued against submicells of defined identity and Holt and Horne (1996) suggested a model in which the casein micelle was presented as a mineralised, cross-linked web of chains of casein molecules that are held together by nanoclusters of calcium phosphate. Horne (1998) suggested a model, called dual binding (poly-condensation) model of the casein micelle. In this model two types of the bonding were postulated: (1) the bonding of individual casein molecules through the hydrophobic regions and (2) linkage of hydrophilic regions (containing phosphoserine clusters) to the colloidal calcium phosphate. The model suggests that the state of association of caseins in the micelles is governed by a balance of attractive hydrophobic interactions and electrostatic repulsion. The effect of temperature, pH and ionic strength on the self-association and calcium-induced aggregation of the individual caseins are explained in terms of their influence on this balance of forces. One method to study these forces is by nanoindentation of casein aggregates in AFM (Helstad et al. 2004; Uricanu et al., 2004).

1.2. Elastic solid properties measured by indentation

Hertz (1881) was the first to study the deformation of elastic bodies in contact. To analyse the force curves obtained from nanoindentation, different models derived from the Hertz model are used. Hertz (1881) described the elastic deformation when two spheres with radii R_1 and R_2 are forced together under a load P.

$$a^3 = \frac{3R_{12}}{4E_r} P \tag{1}$$

or

$$P = \tfrac{4}{3} E_r \sqrt{R_{12}\delta^{3/2}}, \tag{2}$$

where a is the radius of the contact area (m^2); δ the indentation (m); P the load (N); R_{12} a function of R_1 and R_2 (m).

$$1/R_{12} = 1/R_1 + 1/R_2 \tag{3}$$

and E_r is given by

$$\frac{1}{E_r} = \left[\left(\frac{1-\upsilon_1^2}{E_1}\right) + \left(\frac{1-\upsilon_2^2}{E_2}\right)\right], \tag{4}$$

where E_r is the reduced elastic modulus (Pa); E_1 the Young's modulus of sphere 1 (Pa); E_2 the Young's modulus of sphere 2 (Pa); υ_1 the Poisson's ratio of sphere 1; and υ_2 the Poisson's ratio of sphere 2.

Poisson's ratio is the ratio of the contraction strain normal to the applied load divided by the extension strain in the direction of the applied load. The ratio is 0.5 for incompressible material.

Sneddon (1965) developed models for different geometries based on the Hertz model. For small indentations (δ) by a stiff sphere with a radius R on a flat surface the force is given by

$$F = \frac{4E_Y\sqrt{R}}{3(1-\upsilon^2)} \delta^{3/2}. \tag{5}$$

There are variations of this model for different shapes of indenters, e.g. conical:

$$F = \frac{2E_Y \tan\alpha}{\pi(1-\upsilon^2)} \delta^2, \tag{6}$$

where α is the half angle of the cone (°); F the force on the cantilever (N); v the Poisson's ratio of the sample; E_Y the

Young's modulus (Pa); and R the curvature radius of the tip (m).

Domke and Radmacher (1998) measured the elastic properties of thin polymer films with the AFM and used Hertz model to calculate a modulus for the thin layer. In their measurements they could observe that there is a lower limit for the thickness of the layer before the underlying hard surface affects the calculated modulus of the elastic material.

1.3. Liquid droplet deformation

Surface and interfacial tension determine how liquid droplets are shaped when they adhere to a surface as well as how much work is required to increase their interfacial area during deformation. Interfacial tension, γ ($\mathrm{J\,m^{-2}}$) is defined as the Gibbs free energy divided by unit area at constant temperature and pressure. In this system the phases can be considered incompressible and the system to be closed and isothermal. Under these circumstances, changes in Gibbs free energy ΔG, equal to the change in the Helmholtz free energy, are caused by a change in mechanical energy, i.e. work W performed on the system (Kemp, 1984):

$$\Delta G = -\mathrm{d}W. \tag{7}$$

The above work term, $\mathrm{d}W$, is related to deformation of an interface by the fact that in order to produce an infinitesimal increase in the interfacial area, S, an infinitesimal amount of reversible work is required:

$$\mathrm{d}W = -\gamma\,\mathrm{d}S. \tag{8}$$

According to Israelachvili (1992), this can be described by considering Gibbs free energy change or reversible work done, to separate two unit areas from contact to infinity in a vacuum media (labelled 1 and 2, shown in Fig. 1). This is referred to as the work of adhesion, W_{12}. If the two media are identical it is the work of cohesion, W_{33}.The act of creating a new unit area is equivalent to separating two half unit areas from contact, which is also how the surface tension of a media in vacuum is defined (Israelachvili, 1992), thus

$$\gamma_3 = \frac{1}{2}\,W_{33}. \tag{9}$$

Similarly the interfacial tension arising when two immiscible fluids 1 and 2 are in contact, γ_{12}, can be thought of as a two-stage process, first the unit areas of media 1 and 2 are created by the work equal to $\frac{1}{2}W_{11}$ and $\frac{1}{2}W_{12}$. Then they are brought together (negative sign) with a work of $2(\frac{1}{2}W_{12})$ (Israelachvili, 1992), i.e.,

$$\gamma_{12} = \frac{1}{2}W_{11} + \frac{1}{2}W_{12} - W_{12}. \tag{10}$$

This principle can be extended to a 3-phase system, where the work of adhesion of two immiscible phases in a third medium, W_{132}, can be expressed by

$$W_{132} = W_{12} + W_{33} - W_{13} - W_{23} = \gamma_{13} + \gamma_{23} - \gamma_{12}. \tag{11}$$

The work of adhesion can also be used to quantify the contact angle of an adsorbed droplet in an immiscible continuous phase by considering the case shown in Fig. 2. A droplet, D, starts out as spherical, but then settles on the solid flat surface of the solid medium S, becoming a segment of a sphere with one flat section adsorbed to the solid surface where S_{AD} and S_{DS} are the curved and flat areas ($\mathrm{m^2}$) of the droplet shown in Fig. 2, respectively. The contact angle describes the relative size of the interfacial tensions, i.e. solid–droplet (SD) and solid–aqueous (SA) phase interfacial tensions with respect to the aqueous–droplet (AD) phase interfacial tension. Based on Eq. (11) the final Gibbs free energy of this system is

$$W_{\mathrm{tot}} = \gamma_{\mathrm{AD}}(S_{\mathrm{AD}} + S_{\mathrm{DS}}) - W_{\mathrm{ADS}}S_{\mathrm{DS}}. \tag{12}$$

The relative amounts of interfacial area between droplet and the aqueous phase and aqueous phase and the solid will change to minimize the Gibbs free energy. At equilibrium this optimisation process reaches a minimum and can be derived as

$$\gamma_{\mathrm{AD}}(\mathrm{d}S_{\mathrm{AD}} + \mathrm{d}S_{\mathrm{DS}}) - W_{\mathrm{ADS}}\mathrm{d}S_{\mathrm{DS}} = 0. \tag{13}$$

For a droplet of constant volume, where gravity effects are negligible it can be derived geometrically that (Israelachvili, 1992):

$$\frac{\mathrm{d}S_{\mathrm{AD}}}{\mathrm{d}S_{\mathrm{DS}}} = \cos\theta, \tag{14}$$

$$S_{\mathrm{AD}} = \pi(a^2 + h^2), \tag{15}$$

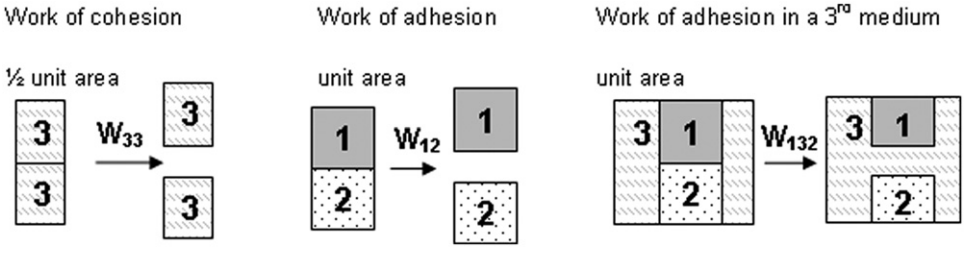

Fig. 1. Schematic diagram showing the principle of work of cohesion and adhesion involving one two and three media (after Israelachvili, 1992).

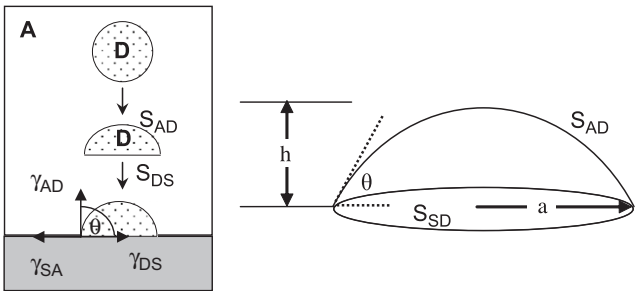

Fig. 2. Droplet geometry is determined by contact angle, which is a result of minimizing the interfacial energy. An initially spherical droplet D, increases its surface area, but decreases in Gibbs free energy when adsorbing to a surface (left, based on Israelachvili, 1992). The relative magnitude of interfacial tensions cause the droplet to obtain a given height, radius and contact angle (right).

$$S_{DS} = \pi a^2, \tag{16}$$

$$\theta = \arccos\left(1 - \frac{h}{2a}\right), \tag{17}$$

where h and a are the height and radius of contact for the adsorbed droplet shown in Fig. 2, respetively.

If a droplet undergoes mechanical deformation by an indenter, the interfacial area is increased, and work (or change in Gibbs free energy) is performed on the droplet which is proportional to the interfacial tension:

$$\Delta G = \gamma_{AD}(\Delta S_{AD} - \cos\,\theta_c \Delta S_{DS}). \tag{18}$$

Through the concept of virtual work, we can solve Eq. (18) for the force, F_{calc}, which would have been required to perform a certain indentation where Δz is the change in tip position, by considering the change in Gibbs free energy:

$$F_{calc} = -\frac{\Delta G}{\Delta z} - \frac{\gamma_{AD}(\Delta S_{AD} - \cos\,\theta_c \Delta S_{DS})}{\Delta z}. \tag{19}$$

The magnitude of the force is determined by how much work is required for each increase in indentation, which is a function of interfacial tension and contact angle and is related to the shape of the AFM tip.

2. Material and methods

2.1. Sample preparation

The whole casein solution (0.02% casein) was prepared from a frozen casein concentrate, produced from micro-filtered, diafiltered and ultrafiltered pasteurised skim bovine milk (22% w/w casein, 0.1% w/w fat, 2.6% w/w lactose, 0.85% w/w calcium, 0.51% w/w phosphorus, supplied by Arla Foods, Stockholm, Sweden). The pH of the concentrate was 6.7, Na-azide (0.2 g kg^{-1}) was added to avoid bacterial growth. Following Horne and Davidson, (1986), the casein concentrate was diluted in a Ca-imidazole buffer (50 mM NaCl, 5 mM $CaCl \cdot 6H_2O$ (Prolabo), 20 mM imidazole, $C_3H_4N_2$ (Merk Darmstadt, Germany)). The pH of the buffer was adjusted to 7.0 using HCl diluted in MilliQ-water. The whole casein solution was prepared 1 d (for one experiment, 6 h), before the AFM imaging and stored at 10 °C. A freshly cleaved graphite surface (HOPG Advanced Ceramics Brand Grade ZYPTM /SPI Supplies, West Chester, PA 19380 USA) was mounted in a fluid cell. Ca-imidazole buffer was injected into the cell for the calibration of the photodiode response to the cantilever against a hard surface. Subsequently, the sample was injected into the cell and allowed to remain there for 2 h before being replaced by 2–3 mL of Ca-imidazole buffer, in which the measurements were performed at approximately 25 °C.

2.2. Instrumentation

The AFM studies were performed with NanoScope III software (Veeco Instruments Inc. Santa Barbara, CA, USA) equipped with a scanner (J-type, maximum scan size 120 μm) and a fluid cell for exchange of buffer and casein solution. NanoScope software version 5.12r3 was used to control the instrument and for data acquisition. Cantilevers used for the measurements were made of silicon nitride, V-shaped, with a spring constant of 0.06 N m^{-1}. The tip shape was square pyramidal, with a tip half angle of 35°. The tips were oxide sharpened (Model # MSCT-AUNM, P/N 00-103-0970, wafer#170-71#19 10/01, (Veeco Instruments Inc. Santa Barbara, CA, USA) MIDAS-computer program, gave a tip radius curvature of 20 nm.

2.2.1. Force measurement AFM

In addition to imaging in contact mode, measurements were also made in "force volume mode". In this mode, force–deformation data are collected over a rectangular grid of points on the investigated surface. In our experiments, data consisting of arrays of 16×16 or 32×32 force curves were recorded with 512 or 256 data points in each force curve. The data were recorded in the relative trigger mode, which ensures that the tip is only pressed with a preset maximum force against the sample. The trigger threshold was set to 240 nm and the deflection sensitivity varied between 70–90 nm V^{-1}. The scan size was 3 μm × 3 μm and the ramp size 600 nm. To obtain a reference of the bare graphite surface for the sensitivity of the photodiode, the first measurements were performed on bare graphite under buffer. Single penetration measurements were made on the same point of a sample to investigate the elastic behaviour of the casein aggregate. The tip velocity for single penetration was 6700 nm s^{-1}. Force volume measurements were preformed at tip velocity that varied from120 to 6700 nm s^{-1}.

2.2.2. Data analysis

The analysis was performed using Matlab 6.1 (The Mathworks Inc. Natic, California, USA). Each force curve consisted of 512 or 256 value pairs of z and d, where z represents the vertical position of the sample holder and d is a measure of the deflection of the cantilever from its zero-force position. For a substrate covered with a layer of

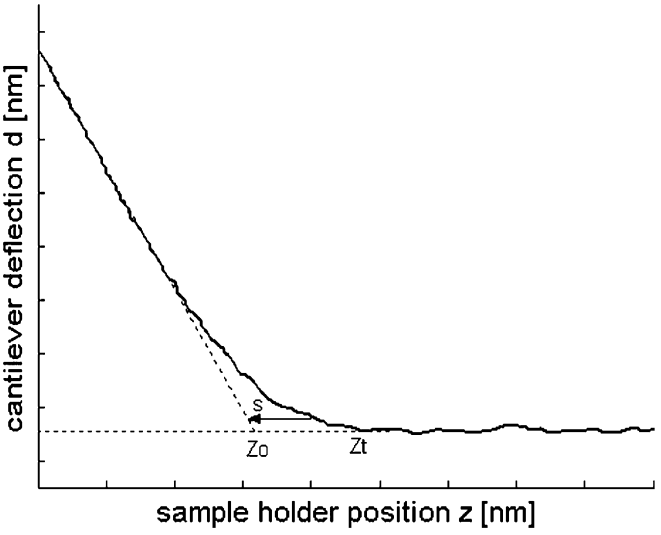

Fig. 3. Definitions of symbols used in data analysis of deflection d vs. sample holder position z.

adsorbed material, AFM does not allow one to assign unambiguously the position of the substrate surface. We have individually least-squares fitted readings in the apparently linear part of the force curves to arrive at the slope $k = -\mathrm{d}d/\mathrm{d}z$ and extrapolated this line to zero force to arrive at a notional position of the hard surface z_0, (Fig. 3). The separation s between the hard surface and the cantilever tip is given by

$$s = z - z_0 + \frac{d}{k}, \tag{20}$$

and the indentation depth δ is given by

$$\delta = z_\mathrm{t} - z_0 - s. \tag{21}$$

2.3. Computer modelling of surface tension phenomena

To interpret the observed liquid droplet behaviour of the adsorbed casein aggregate, the surface tension phenomena were explored by computer modelling using the Surface Evolver. The Surface Evolver is a public domain finite element package, which was developed by Ken Brakke as part of an American National Science Foundation funded geometry supercomputing project. It is an interactive program for the study of interfaces shaped by surface tension and other energies, subject to various constraints. The user defines an initial interface in a data file. The program then evolves the interface, minimising its energy using a gradient descent method. The numerical algorithm based on Lagrange's principle of virtual work, stating that a mechanical system in a state of equilibrium has a minimum in the system's total energy (Brakke, 1992). It is generally used for solving problems involving the minimization of surfaces (Brakke, 1992, 1996) with practical applications in the design of solder joints for microchips (Zhu, Wang, & Lou, 1998), prediction of the wetting of fibres (McHale & Newton, 2002), controlled production of liquid pillars used for pharmaceutical drug screening (Silver et al., 1999), and prediction of droplet sizes in membrane emulsification (Rayner, Trägårdh, & Trägårdh, 2005; Rayner, Trägårdh, Trägårdh, & Dejmek, 2004).

The Surface Evolver uses a triangular tessellation of facets (or mesh) to represent interfaces which can be increasingly refined to achieve the desired level of accuracy. The Surface Evolver parameterises interfaces in terms of its vertex co-ordinates for a particular triangulation and then modifies a given initial interface shape taking into account the requirements of the Gauss–Laplace equation. The shape of the adsorbed droplet (or adsorbed aggregate) under a certain set of constraints is found by iteratively moving vertices using the Newton–Raphson method to quickly converge to a local minimum (Bradley & Weaire, 2001). The code automatically takes into account the contributions of the interface to the system's energy, whereas the shape of the boundaries and their wetting energies have to be added by the user by providing appropriate integration coefficients along the contact lines (Brakke, 1992).

The effect of surface tension and wetting energy is modelled by considering the relative wetting energy via the geometrically calculated contact angle from height versus volume data using Eq. (17). This contribution is modelled by giving the edge in contact with the surface an energy integrand (Brakke, 1992). Let S be the orientated droplet surface in contact with the surface, T the contact energy density and $\mathbf{i}$, $\mathbf{j}$, and $\mathbf{k}$ the unit basis vectors in the directions x_1, x_2 and x_3. Then we want to find a vector field $\mathbf{B}$ such that

$$\int_{\text{contact } \mathbf{area}} T\mathbf{k} \cdot \mathrm{d}\mathbf{S} = \int_{\text{contact } \mathbf{line}} \mathbf{B} \cdot \mathrm{d}\mathbf{l}. \tag{22}$$

$T = (-\cos(\theta \times \pi/180))$, θ is the interior angle between plane and surface, and $\mathbf{l}$ is the length of the contact line (Brakke, 1992).

Now by using Stokes' Theorem

$$\operatorname{curl} \mathbf{B} = T\mathbf{k} \text{ and thus we can use } \mathbf{B} = -Tx_2\mathbf{i}. \tag{23}$$

This gives the contact energy in the form of a line integral around the contact line which is constrained to lie on the graphite surface at $x_3 \leqslant 0$.

2.3.1. Force curves from interfacial tension

The simulated droplet in Surface Evolver obtains its shape by minimizing its interfacial free energy taking into consideration the relative interfacial tensions of the surface–droplet and droplet–aqueous areas. Using the Surface Evolver the tip shape is defined via constraints. The tip is constructed as a boundary in space where the droplet interface may not exit. This will cause the interface to deform to meet the constraint and thereby an increase in interfacial energy used to calculate the equivalent force required for the deformation from Eq. (19). It is assumed

that the energy contribution from the tip indentation is determined solely by the forced increase in droplet area.

2.3.2. Modelling the AFM tip in the surface evolver

The AFM tip is defined by two geometric parameters, the curvature at the apex and the opening angle of the pyramid. The curvature at the apex is defined by the manufacturer as the cross-sectional diameter of the pyramid at 5 nm below the apex. The curvature value provided for the AFM tip used in this study was 14–20 nm (Veeco Instruments Inc. Santa Barbara, CA, USA). The opening angle is the slope of the pyramid's sides, and is 70° ($\phi = 35°$ for the right-angle triangle) shown in Fig. 4. In the Surface Evolver simulation the tip is modelled as a boundary in space where the tip and the adsorbed casein aggregate interface modelled as the mesh cannot co-exist. This boundary is defined in such a way that it can be moved vertically to indent the simulated casein aggregate, and horizontally to allow indentations at different starting positions. This boundary is defined by the following equation:

$$(x_1 - x_{\text{pos}})^{rq} + (x_2 - y_{\text{pos}})^{rq} = (\tan\ \phi(x_3 - x_{\text{tip}}))^{rq} \qquad (24)$$

where x_1, x_2, x_3 are Cartesian position coordinates in the Surface Evolver, x_{pos} and y_{pos} are the offset in the x_1 and x_2 directions, respectively, from the centre of the simulated aggregate lying at the origin. Here ϕ is the half open angle, z_{tip} is the position of the tip apex which moves in the negative x_3 direction during indentation. rq is the super-elliptical exponent which determines the sharpness of the corners of the pyramid. For a schematic of the tips boundary see Fig. 4. In this model rq was equal to 8 because increasing the sharpness corner further did not give significantly different results with the level of mesh refinement used.

2.3.3. Assumptions made in the Surface Evolver model

1. Constant interfacial tension and contact angle (assumed equilibrium).
2. No effects from inertia, viscous dissipation, gravitation, or kinetic energy.
3. The adsorbed casein aggregate did not slide on the graphite surface, $\Delta S_{\text{DS}} = 0$.
4. The interfacial tension between the indenter and aggregates is equal to the interfacial tension between the aqueous phase and the aggregate, γ_{AD} (no adhesion).

The first two assumptions are founded on the experimental observations that the measured aggregate stiffness was independent of indentation speed (i.e., no viscous or elastic effects) and the same result was obtained for repeated indentation in the same position (the surface achieved rapid re-equilibration). The third assumption was necessary for the calculation and is based on the fact that if the adsorbed casein aggregate did slide significantly it would not have been possible to measure by AFM. The fourth assumption is supported by the experimental findings which showed no difference in the measured force during indentation and retraction of the tip.

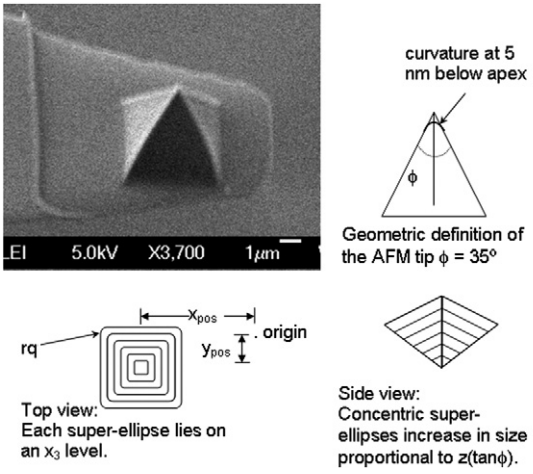

Fig. 4. SEM-image of a cantilever with a pyramidal 20 nm-radius tip. (Images courtesy Dr Jacob Wagner) top left; schematic of geometric parameters and tip boundary defined by Eq. (24) right and bottom

2.3.4. Constraints and their energy contribution in the surface evolver model

The casein aggregate has a constant volume existing $x_3 \geqslant 0$.

The edge in contact with the graphite surface at $x_3 = 0$ has an energy contribution calculated using the energy integrand for the line integral in Eq. (22).

The surface casein aggregate cannot intersect the boundary described by

$$(x_1 - x_{\text{pos}})^{rq} + (x_2 - y_{\text{pos}})^{rq} = (\tan\ \phi(x_3 - x_{\text{tip}}))^{rq} \leqslant 0. \qquad (25)$$

2.3.5. Calculation procedure for the surface evolver simulation

The tip boundary is first moved towards the aggregate surface (negative x_3 direction) until it touched. The aggregate surface is then indented by the tip boundary by decreasing the value of z_{tip} in small steps ($z_{\text{tip}} = z_{\text{tip}} - 0.001h$). At each step the surface is forced to deform to comply with constraint 3. This deformation increases the area of the casein aggregates interface, which in turn increases the Gibbs free energy. This energy is higher than that of the non-deformed surface and is calculated numerically by the Surface Evolver.

After each tip movement, a gradient descent is performed to obtain the surface configuration of lowest Gibbs free energy for that particular tip position and given set of constraints; the surface area, volume, and total energy are calculated. The results from each step are written to the output file and the next tip movement occurs. This process iterates until the tip fully indents the casein aggregate, $z_{\text{tip}} = 0$.

The data from the Surface Evolver was plotted in Matlab and the force was calculated from the change in energy as a function of indentation using Eq. (19). The model used in the Surface Evolver simulations has one unknown parameter, namely the magnitude of the interfacial tension γ_{AD} (in Eq. (18)). The geometric analysis of the aggregate radius versus height data only yields the contact angle, which describes the relative size of the graphite–casein aggregate interfacial tension with respect to the aqueous–casein aggregate interfacial tension. For this reason one of the tensions must be assumed for the calculations to have dimensions.

3. Results and discussion

3.1. Topographic height images

Casein adsorbed onto graphite surface under Ca–imidazole buffer, pH 7, either as a thin layer, with a thickness of some 10–15 nm or as aggregates. As seen in the AFM images (height data) in Fig. 5, the aggregates were affected by the graphite surface and had a shape of a section of a spherical cap rather than a sphere. It is known that casein micelles, or fragments of them bind well to, and stabilize, liquid hydrophobic materials, (Dalgleish, West, & Hallett, 1997) because the hydrophobic interior of the micelle is exposed and binds to the substrate. Particles adsorbed in this way experience a spreading pressure (Dalgleish et al., 2004). It could not be determined whether the adsorbed aggregates were actually formed on the graphite surface, or if they were adsorbed from the micellar solution, however, the volume of the adsorbed aggregates was calculated and found to be of the same order of magnitude as the volume of native casein micelles. The aggregates appear smooth, however, the apparent surface is inherently smoothed, corresponding to a rolling ball smoothing algorithm with a ball of 20 nm radius.

Fig. 6 shows the ratio between the height and diameter for the attached aggregates on a hydrophobic graphite surface (solid line) and the results presented by Uricanu et al. (2004), for casein micelles (dotted line), attached onto a functionalised gold-covered glass slide. The ratio between the height and diameter was linear in both cases. However, the adsorbed casein aggregates on a hydrophobic graphite surface had a flatter shape, compared to the casein micelles on the functionalised surface which were almost spherical. The linear ratio between the casein aggregate diameter and height indicates a constant contact angle and thus liquid droplet like behaviour. Using Eq. (17) the

Fig. 5. Casein aggregates on a hydrophobic graphite surface. Scan size 3000×3000 nm. Height scale 400 nm. The height of casein aggregate A is 110 nm and the diameter is 680 nm.

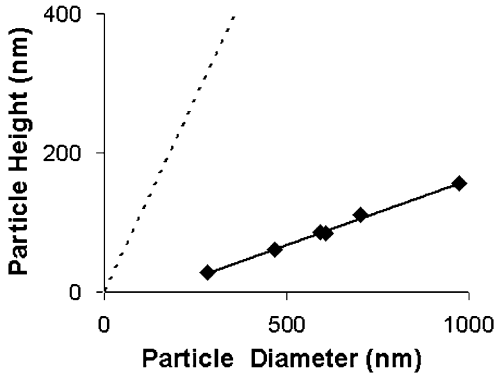

Fig. 6. Height and diameter of adsorbed aggregates. The solid line shows the ratio between heights vs. diameter for 11 aggregates. The dotted line shows the ratio for relative height and width for the casein micelles attached by a functionalised gold surface (Uricanu et al., 2004).

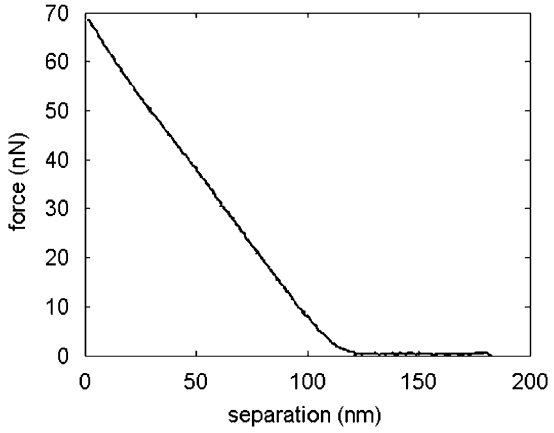

Fig. 7. A typical force vs. separation curve from an indentation into the centre of an aggregate.

casein aggregate–graphite contact angles were calculated, having an average $30^\circ \pm 8\%$CV, $n = 11$.

3.2. Force curves

3.2.1. Analysis of time-dependent behaviour

To get an impression how the shape of the force vs. indentation curves correlated with the different size and shape of the casein aggregates, 110 force versus separation curves from 26 different casein aggregates, attached to the graphite surface, were carefully analysed. The force curves were measured during three different experiments and the repeatability of the experiments was good. The separation and force were calculated from the deflection vs. sample holder position curves. Fig. 7 shows a typical force curve from an indentation performed at the centre of an aggregate. We obtained almost identical curves on approach and retraction, thus the changes brought about by the tip were reversible on the 0.1-s scale. None of the curves showed any regular discontinuities, and thus no evidence of a substructure at tens of nanometers scale was

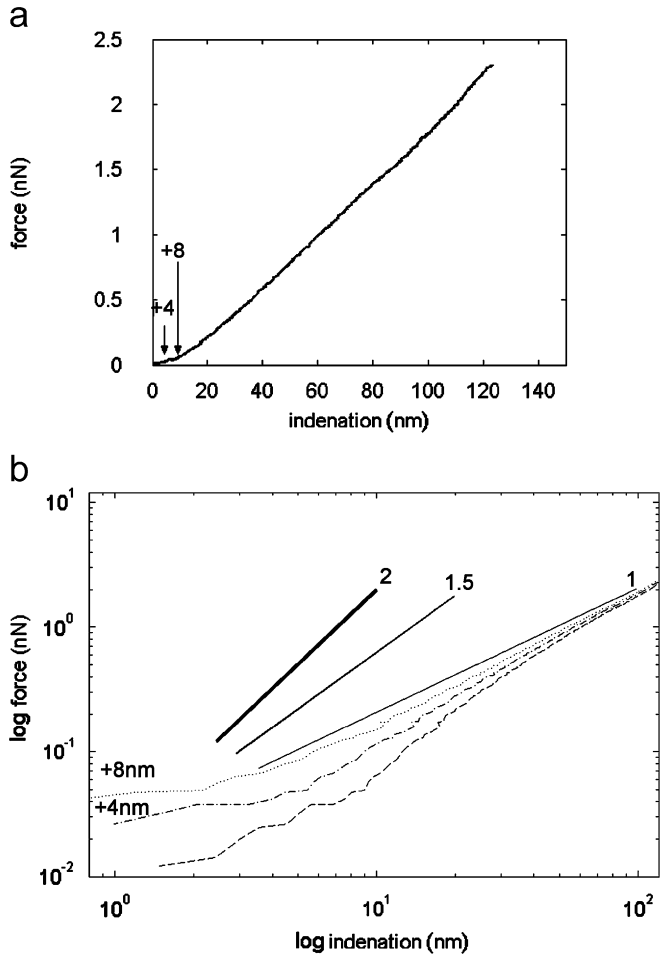

Fig. 8. (a) The force vs. indentation curve plotted (indentation start from zero). +4 and +8 show the points for the different touch points. (b) Log force vs. log indentation, for three different touch points, dashed line: chosen touch point 1; dash-dot line: touch point 1+4 nm, dot-line: touch point 1+8 nm. The solid lines present a slope of 2 (expected for pyramid), 1.5 (expected for sphere) and 1 (expected for linear).

observed. Two single penetrations at the same point with a tip velocity of (6700 nm s^{-1}), produced force curves with the same slope and the same contact point. The time between the indentations was about 10 s. No changes in the structure could be detected in the second or subsequent penetrations. Further more, measurements were made at three different tip velocities (120, 1200 and 6700 nm s^{-1}). On the probed time scale there was no evidence of viscous or viscoelastic behaviour. The deformation rate $(\Delta h/h_0)/\Delta t$ for these samples varied between 0.8 and 41.9 s^{-1}. The deformation rate is in the same range as for common rheological measurements for casein gels and cheese products. In casein curd, a change of some 30% in modulus would have been expected (Zoon, van Vliet, & Walstra, 1988). In addition no increase in force was detected when the tip approached the hard surface as would have been expected if the aggregate had properties like that of an elastic solid (Domke & Radmacher, 1998).

3.2.2. Force curves and Hertz model

The force curves were recalculated from force vs. separation curves to force vs. indentation curves (Eq. (21)). In logarithmic coordinates, the force vs. indentation relation of an elastic solid indented by our tip would be expected to exhibit a slope of 1.5 (appropriate for a sphere) for about the first 15 nm, and gradually change to an asymptotical slope of 2 corresponding to the behaviour of the pyramidal indenter (Eqs. (5) and (6)). However this was not the case, Fig. 8(a). The early part of the force deformation curve may not be representative of the bulk properties of the aggregate—this is implicit in all the proposed models of casein micelle structure. It is likely that in at least the first 5–10 nm from the apparent surface, the average density of the protein chains is lower than in the bulk of the aggregate (as in the "hairy layer" of native casein micelles). However shifting the position of the

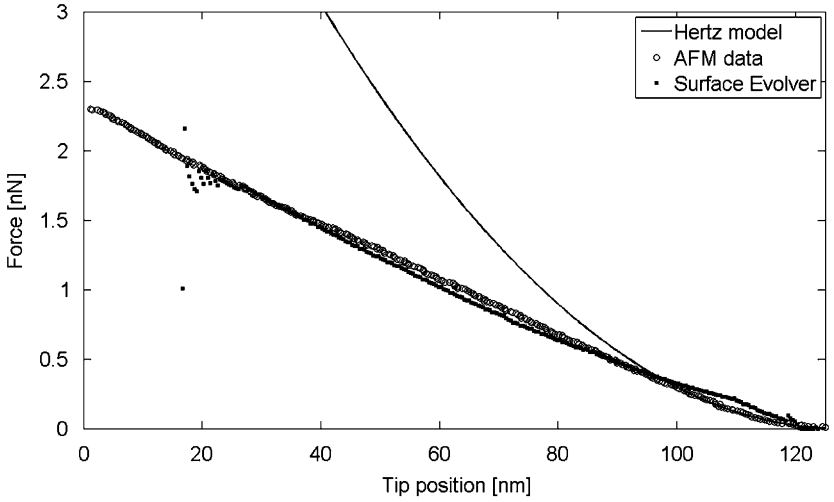

Fig. 9. Comparison of the Hertz Model and Surface Evolver simulations to AFM data.

touch point to compensate for the surface layer introduces arbitrariness which dramatically affects any data fitting, this is demonstrated in Fig. 8(b) for a shift of 4 or 8 nm. The asymptotical behaviour on the other hand is hardly affected, and there can be no doubt that the asymptotic behaviour did not agree with a slope of 2. From the results presented above, we may conclude that the adsorbed casein aggregates did not behave like an elastic solid. To find an explanation to the force curve shapes, a surface tension based model was explored using Surface Evolver.

3.3. Surface tension based model

A surface tension based model essentially postulates that internal rearrangements in the aggregate occur at a timescale significantly shorter than the timescale of deformation, and that the energy expenditure for deformation scales with the increase of the interfacial area. This is plausible if the cohesion of the aggregate is primarily determined by bonds with 'low' energy content, e.g. hydrophobic interactions between short stretch of hydrophobic entities. As we indent the casein aggregate we change the area/volume ratio of the aggregate and therefore also the composition of the surface. In our experiments, the liquid-facing area expanded by some 30%. The κ-casein is predominantly present at the external surface of casein micelles, covering about one third of it, (Dalgleish, Horne, & Law, 1989), and when the surface is increased the surface κ-casein concentration will decrease. However, β-casein is more surface active than κ-casein and the maximum surface pressures of the individual caseins do not differ much, (Mulvihill & Fox, 1989), and thus there is no reason to expect any pronounced effect of the deformation induced surface composition change on the apparent surface tension in our model.

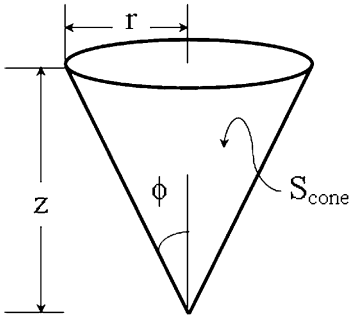

Fig. 10. Simplified cone geometry.

3.4. Surface evolver simulation

Simulation results from the Surface Evolver, as seen in Fig. 9 correctly predict the linear characteristic of the force curves obtained by AFM measurements. As stated earlier, the aggregate–buffer interfacial tension is not known à priori, but is a scalar constant in the calculated force in Eq. (19). From analysis of the magnitude of the experimental force curves the aggregate–buffer interfacial tension was estimated to be of the order of 10 mJ m^{-2} and this is the value used in all reported simulations. Furthermore, there was also found a vertical offset between the point at which the AFM tip began to interact with the aggregate in the experimental data and the height at which the simulated indenter in the Surface Evolver begins to deform the surface. This distance was 8 to 15 nm, which is comparable to the thin layer of casein reported in Helstad et al. (2004).

Fig. 9 also compares the Surface Evolver simulation predicting the force vs. indentation to what the Hertz model would have given. The roughly linear shape of the force versus indentation curves obtained from the liquid droplet model implemented in the Surface Evolver can be explained by following argument.

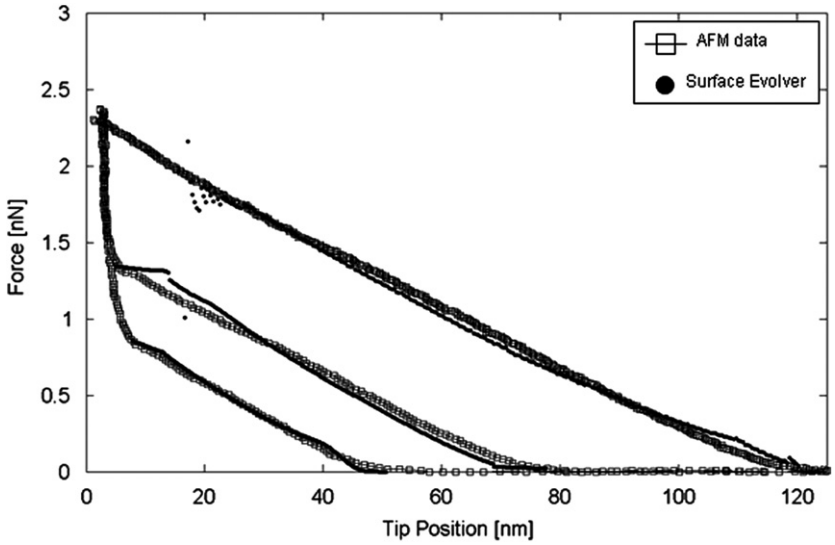

Fig. 11. AFM data and Surface Evolver Simulations of three different sized aggregates. Indentation in centre, $\gamma_{AD} = 10\,mJ\,m^{-2}$.

The surface area of the pyramidal indenter used in this study increases linearly with distance from the apex (neglecting the first 5 nm where it is rounded), for this reason we can explain the occurrence of linear force curves geometrically using the case of a simple cone (see Fig. 10). The surface area of a cone as a function of its height z is given by

$$S_{\text{cone}} = \pi r\sqrt{r^2 + z^2}, \tag{26}$$

where r and z are related by the half-opening angle, ϕ:

$$r = \tan\phi\, z, \tag{27}$$

$$S_{\text{cone}} = \pi \tan\phi\, z\sqrt{(\tan\phi\, z)^2 + z^2} = z^2\pi \tan\phi\sqrt{(\tan\phi)^2 + 1}. \tag{28}$$

Thus;

$$S_{\text{cone}} \propto z^2. \tag{29}$$

If we assume that the increase in the interfacial area is proportional to the amount of displaced surface area of the cone then

$$\mathrm{d}E = \gamma\,\mathrm{d}A \approx \gamma S_{\text{cone}} \propto z^2. \tag{30}$$

By taking the derivative of E with respect to z we find that the force is equal to a proportionality constant times z:

$$F = \frac{\mathrm{d}E}{\mathrm{d}z} = \frac{\mathrm{d}(z)^2}{\mathrm{d}z} \propto z. \tag{31}$$

Thus the force vs. indentation curves are straight lines as shown in Fig. 9.

The value of surface tension ($10\,\mathrm{mJ\,m^{-2}}$), is low compared to a protein stabilized air bubble but high compared to an aqueous two phase system. We have not been able to find published surface tension data on any similarly hydrated proteinaceous aggregate. An indirect comparison could be made with cubosomes, bicontinuous liquid crystalline nanoparticles with high water content. These are typically based on monoglyceride, water and pluronic F127, but can also be stabilized by caseinate instead of the block surfactant, (Buchheim & Larson, 1987). The apparent surface tension of cubosomes can be estimated from the energy input needed to produce small particles. Microfluidisation at 345 bar gave rise to cubosomes of on average 100 nm diameter, (Barauskas, Johnsson, Joabsson, & Tiberg, 2005), where milk fat at comparable microfluidising conditions, (Tosh and Dalgleish, 1998), gave some 350 nm. With $27\,\mathrm{mN\,m^{-1}}$ for the surface tension of clean oil-water interface, the apparent surface tension of cubosomes could be estimated to be some $8\,\mathrm{mN\,m^{-1}}$, which makes our result plausible.

3.5. Different aggregate sizes

A typical example of the forces measured when indenting the centre of aggregates of different sizes, is presented in Fig. 11. The liquid droplet-like behaviour, modelled in the Surface Evolver simulations which assume a constant interfacial tension, showed good agreement with the measured force curves as shown.

The stiffness of the casein aggregates seemed to be independent of their size. This result differed from the result presented by Uricanu et al. (2004). In their system, the modulus of the casein aggregates increased with an increased aggregate size, and the effect was proposed to be caused by size-dependent compositional differences of casein micelles. The systems are however not directly comparable. In their study, spherical native casein micelles were attached via carbodiimide chemistry to a functionalised substrate whereas in ours, the casein aggregates

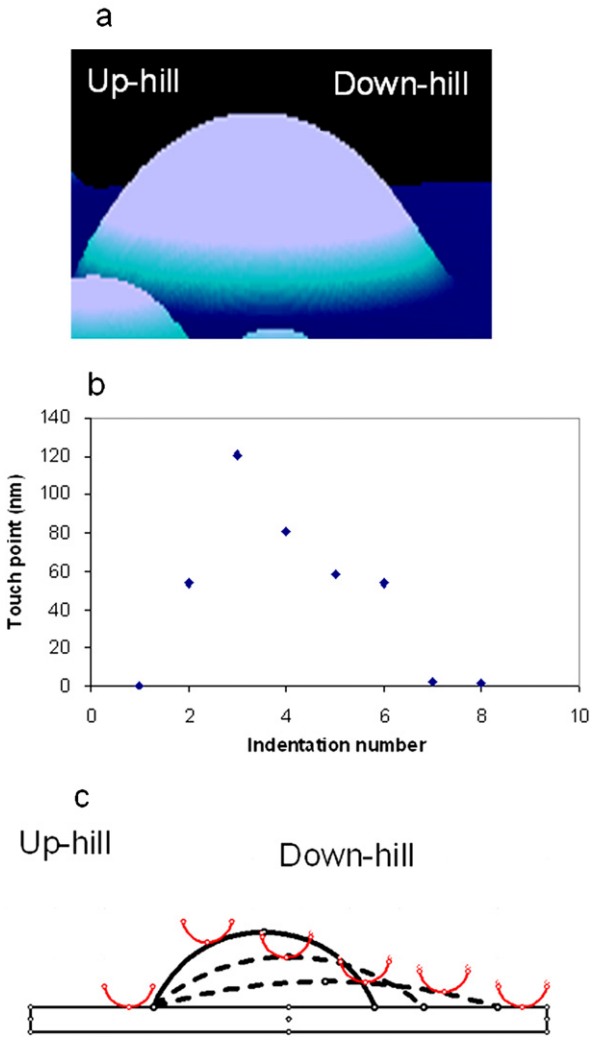

Fig. 12. Scan direction and apparent images of adsorbed aggregate. (a) Aggregate A, a spherical cap shape in topographic image. (b) A height profile of the aggregate from touch points obtained from the force curve array (force volume), scan direction from left to right. (c) Original shape of aggregate (solid line), and apparent touch points as affected by spreading of the aggregate (dashed) as a consequence of successive indentations from left to right.

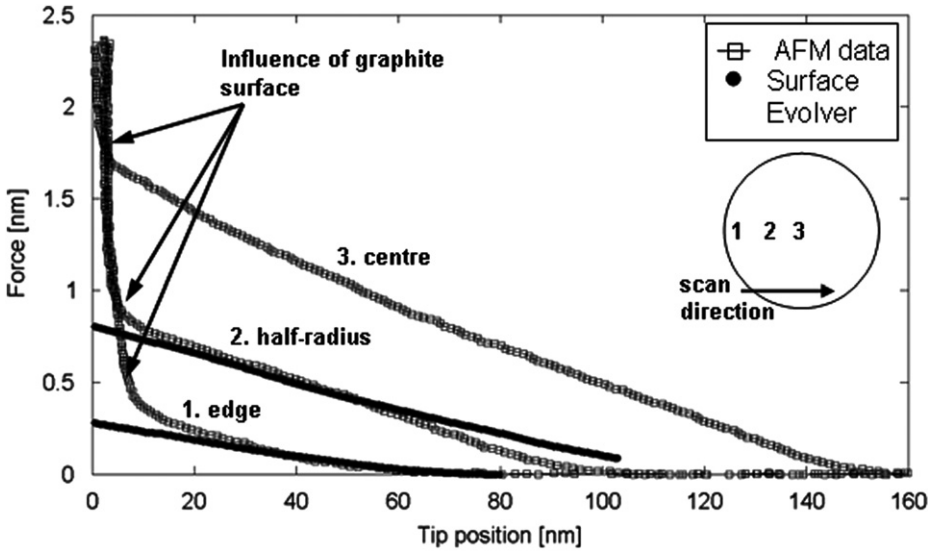

Fig. 13. AFM data and Surface Evolver simulations of different positions on aggregate. Scan direction and relative position on aggregate are shown in the inset right.

lacked the calciumphosphate of native casein and were adsorbed to the solid surface by partial wetting. The presence of rigid calcium phosphate nanoclusters is at least comparable to the presence of well bonded rigid filler in a homogeneous composite, which would be expected to give rise to a more stiff system. The effect may even be much larger if the calcium phosphate nanoparticles constitute a part of the rheologically active gel backbone.

3.6. Off-centre indentation

Different behaviour was observed on the "uphill" face of the aggregate, i.e. the face that was first subject to indentations, see Fig. 12, and the "downhill" face. On the "uphill" face of the aggregate, the apparent touch points as observed in force mode agreed reasonably well with the aggregate contour of the topographic mode (Fig. 12(a)). The surface tension based model described correctly the observed apparent softening (decreased force curve slope) for the off-centred indentations, Fig. 13. Similar off-centre softening was also found by Uricanu et al. (2004). They report a decrease in relative Young's modulus E^* for casein micelles from 400 kPa at the apex to 200 kPa at a 50 nm offset towards the periphery of a micelle 270 nm in diameter.

The apparent position of the touch points further in the scanning direction ("downhill") was unsymmetrical as shown in Fig. 12(b). One possible explanation could be that the aggregate is being displaced by the repeated indentations on the uphill face so that it spreads in the scan direction, as illustrated schematically in Fig. 12(c). The downhill off-centre indentation gave a stiffer behaviour, Fig. 14. The spread molecules could have different affinities to the interfaces than the bulk of the original aggregate, and thus give rise to changed indentation behaviour. Some

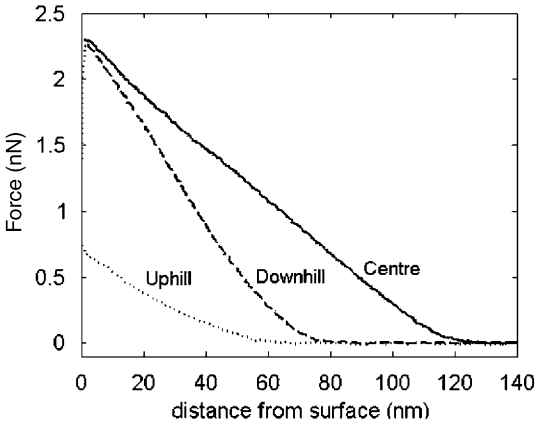

Fig. 14. Observed scan-direction-dependent differences.

additional effect could be caused by buckling of the cantilever, which differs between the uphill and downhill faces, Fig. 15.

4. Conclusions

The results indicate that a surface tension based model, rather than one based on a uniform elastic solid, can successfully describe many key characteristics of the nanorheological behaviour during deep indentation of casein aggregates absorbed from a diluted whole casein solution onto a hydrophobic surface. This indicates that the interactions involved in the aggregation of Ca-phosphate depleted casein are relatively weak, and weak hydrophobic interactions probably play an important role.

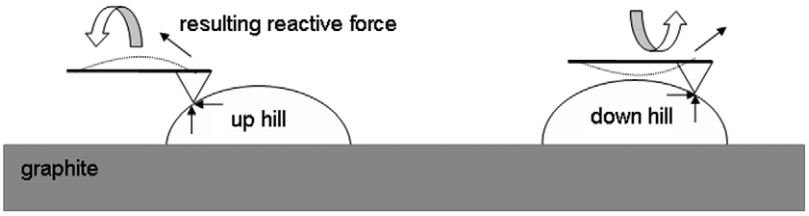

Fig. 15. Schematic of the effect of buckling of the cantilever on the measured force.

Acknowledgement

The Danish Dairy Research Foundation supported this study.

References

Aoki, T., Yamada, N., & Imamura, T. (1988). Dissociation during dialysis of casein aggregates cross-linked by colloidal calcium-phosphase in bovine casein micelles. *Journal of Dairy Research*, *55*(2), 189–195.

Barauskas, J., Johnsson, M., Joabsson, F., & Tiberg, F. (2005). Cubic phase nanoparticles (cubosome): Principles for controlling size, structure, and stability. *Langmuir*, *21*(6), 2569–2577.

Bradley, G., & Weaire, D. (2001). Instabilities of two liquid drops in contact. *Computing in Science and Engineering*, *3*(5), 16–21.

Brakke, K. A. (1992). The surface evolver. *Experimental Mathematics*, *1*(2), 141–165.

Brakke, K. A. (1996). The surface evolver and the stability of liquid surfaces. *Philosophical Transactions of the Royal Society of London, Series A: Mathematical Physical and Engineering Sciences*, *354*(1715), 2143.

Buchheim, W., & Larson, K. (1987). Cubic lipid–protein–water phases. *Journal of Colloid and Interface Science*, *117*(2), 582.

Dalgleish, D. G. (1984). Measurement of electrophoretic mobilities and zeta-potentials of particles from milk using laser Doppler electrophoresis. *Journal of Dairy Research*, *51*(3), 425–438.

Dalgleish, D. G. (1998). Casein micelles as colloids: Surface structures and stabilities. *Journal of Dairy Science.*, *81*(11), 3013–3018.

Dalgleish, D. G., Horne, C., & Law, A. J. R. (1989). Size-related differences in bovine casein micelles. *Biochemica et Biophysica Acta*, *991*(3), 383–387.

Dalgleish, D. G., Spagnuolo, P. A., & Goff, H. D. (2004). A possible structure of the casein micelle based on high-resolution field-emission scanning electron microscopy. *International Dairy Journal*, *14*(12), 1025–1031.

Dalgleish, D. G., West, S., & Hallett, F. R. (1997). The characterization of small emulsion droplets made from milk proteins and triglyceride oil. *Colloids and Surfaces A: Physicochemical and Engineering Aspects*, *123*, 145–153.

De Kruif, C. G., & Holt, C. (2003). Casein micelle structure, functions and interactions. In P. F. Fox, & P. L. H. McSweeney (Eds.), *Advanced dairy chemistry—1: proteins, Part A*, vol. 1 (pp. 233–276). New York: Kluwer Academic Publishers.

Domke, J., & Radmacher, M. (1998). Measuring the elastic properties of thin polymer films with the atomic force microscope. *Langmuir*, *14*(12), 3320–3325.

Helstad, K. M., Braem, A. D., Trckova, J., Paulsson, M., & Dejmek, P. (2004). Nanorheological properties of casein. In E. Dickinson (Ed.), *Food colloids; interactions, microstructure and processing* (pp. 218–229). London, England: Royal Society of Chemistry.

Hertz, H. J. (1881). Ueber die Berührung fester elastischer Körper. *Journal für die reine und angewandte Mathematik*, *92*, 156–171.

Holt, C. (1992). Structure and stability of bovine casein in micelles. In C. B. Anfinsen, J. T. Edsall, D. S. Eisenberg, & F. M. Richards (Eds.), *Advances in protein chemistry* (pp. 63–151). New York: Academic Press.

Holt, C., & Horne, D. S. (1996). The hairy casein micelle: Evolution of the concept and its implications for dairy technology. *Netherlands Milk and Dairy Journal*, *50*(2), 85–111.

Horne, D. S. (1998). Casein interactions: Casting light on the black boxes, the structure of dairy products. *International Dairy Journal*, *8*(3), 171–177.

Horne, D. S., & Davidson, C. M. (1986). The effect of environmental conditions on the steric stabilization of casein micelles. *Colloid and Polymer Science*, *264*(8), 727–734.

Israelachvili, J. N. (1992). *Intermolecular and surface forces*. London: Academic Press.

Kemp, H. R. (1984). The concept of energy without heat or work. *Physics Education*, *19*, 234–235.

Lucey, J. A., Dick, C., Singh, H., & Munro, P. A. (1997). Dissociation of colloidal calcium phosphate-depleted casein particles as influenced by pH and concentration of calcium and phosphate. *Milk Science International*, *52*(11), 603–606.

McHale, G., & Newton, M. I. (2002). Global geometry and the equilibrium shapes of liquid drops on fibers. *Colloids and Surfaces A*, *206*(1-3), 79–86.

Mulvihill, D. M., & Fox, P. F. (1989). Physico-chemical and functional properties of milk proteins. In P. F. Fox (Ed.), *Developments in Dairy Chemistry—4, Functional milk proteins*. London and New York: Elsevier Applied Science.

Rayner, M., Trägårdh, G., & Trägårdh, C. (2005). The impact of mass transfer and interfacial expansion rate on droplet size in membrane emulsification processes. *Colloids and Surfaces A*, *266* (1-3), 1–17.

Rayner, M., Trägårdh, G., Trägårdh, ., & Dejmek, P. (2004). Using the Surface Evolver to model droplet formation processes in membrane emulsification. *Journal of Colloid Interface Science*, *279*(1), 175–185.

Schmidt, D. G. (1980). Colloidal aspects of casein. *Netherlands Milk Dairy Journal*, *34*(1), 42–64.

Schmidt, D. G. (1982). Association of caseins and casein micelle structure. In P. F. Fox (Ed.), *Advanced Dairy Chemistry 1, Proteins* (pp. 61–85). London: Applied Science Publishers.

Schmidt, D. G., & Payens, T. A. J. (1976). In E. Matijevic (Ed.), *Surface and Colloids Science*, vol. 9 (pp. 129–165). New York: Wiley.

Silver, J., Mi, Z. H., Takamoto, K., Bungay, P., Brown, J., & Powell, A. (1999). Controlled formation of low-volume liquid pillars between plates with a lattice of wetting patches by use of a second immiscible fluid. *Journal of Colloid Interface Science*, *219*(1), 81–89.

Slattery, C. W., & Evard, R. (1973). Model for formation of casein micelles from subunits of variable composition. *Biochimica et Biophysica ACTA*, *317*(2), 529–538.

Sneddon, I. N. (1965). The relation between load and penetration in the axisymmetric Boussinesq problem for a punch of arbitrary profile. *International Journal of Engineering Science*, *3*, 47–57.

Tosh, S. M., & Dalgleish, G. G. (1998). The physical properties and renneting characteristics of the synthetic membrane on the fat

globules of microfluidized milk. *Journal of Dairy Science*, *81*, 1840–1847.

Uricanu, V. I., Duits, M. H. G., & Mellema, J. (2004). Hierarchical networks of casein proteins: An elasticity study based on atomic force microscopy. *Langmuir*, *20*(12), 5079–5090.

Walstra, P. (1979). Voluminosity of bovine casein micelles and some of its implications. *Journal of Dairy Research*, *46*(2), 317–323.

Walstra, P. (1990). On the stability of casein micelles. *Journal of Dairy Science*, *73*(8), 1965–1979.

Walstra, P. (1999). Casein sub-micelles: Do they exist? *International Dairy Journal*, *9*(3–6), 189–192.

Walstra, P., Geurts, T. J., Noomen, A., Jellema, A., & van Boekel, M. A. J. S. (1999). *Dairy tehcnology: Principles of milk properties and processes*. New York: Marcel Dekker.

Zhu, Q., Wang, G., & Lou, L. (1998). Optimization of design and manufacturing parameters for solder joint geometry and self-alignment in flip-chip technology. In *Proceedings of the fifth international conference on solid-state and integrated circuit technology. The Hague, October 1998* (pp. 554–558). Piscataway, NJ: IEEE.

Zoon, P., van Vliet, T., & Walstra, P. (1988). Rheological properties of rennet induced skim milk gels. 2. The effect of temperature. *Netherlands Milk Dairy Journal*, *42*, 271–294.